Title:

Structural and magnetic investigation of Fe^{3+} and Mg^{2+} substitution into the trigonal bipyramidal site of $InGaCuO_4$

Author Affiliations:

Rosa Grajczyk, Romain Berthelot, Sean Muir, A. W. Sleight and M. A. Subramanian*
Department of Chemistry, Oregon State University, Corvallis, OR 97331

*Corresponding author: mas.subramanian@oregonstate.edu

Full Email Addresses:

Rosa Grajczyk	rabinovr@onid.orst.edu
Romain Berthelot	berthelot@icmcb-bordeaux.cnrs.fr
Sean Muir	muir.sean@gmail.com
A. W. Sleight	arthur.sleight@oregonstate.edu
M. A. Subramanian	mas.subramanian@oregonstate.edu

Corresponding Author:

Mas Subramanian
mas.subramanian@oregonstate.edu
153 Gilbert Hall
Department of Chemistry, Oregon State University
Corvallis, OR 97330 U.S.A

Tel: 1-541-737-8235

Abstract:

The solid solutions of $InGa_{1-x}Fe_xCuO_4$, $InFeCu_{1-x}Mg_xO_4$, and $InGa_{1-x}Fe_xCu_{1-x}Mg_xO_4$ were synthesized and characterized through the use of X – ray and neutron diffraction, and DC – magnetism measurements. All compositions of $InGa_{1-x}Fe_xCuO_4$ are single phase and crystallize in the $R\bar{3}m$ space group, but a transformation to the spinel $InFeMgO_4$ structure was observed for the other series of Fe^{3+} and Mg^{2+} − rich compounds. As a result of the similar ionic radii for Ga^{3+} and Fe^{3+}, there was not an obvious change in the *c/a* ratio for $InGa_{1-x}Fe_xCuO_4$. In the hexagonal domains, the *c/a* ratio of $InFeCu_{1-x}Mg_xO_4$ and $InGa_{1-x}Fe_xCu_{1-x}Mg_xO_4$ showed a linear trend that can be explained by the change in electronic configurations between Cu^{2+} and Mg^{2+}. All hexagonal compositions display negative Weiss temperatures, and there is an increase in the magnetic transition temperature with the addition of Fe^{3+}. Additional AC magnetic susceptibility measurements for the x = 0.4 and 0.6 compositions within the $InGa_{1-x}Fe_xCuO_4$ solid solution show that these transitions are consistent with spin glass behavior, not long range AFM ordering.

Keywords: Transition metal oxides, trigonal bipyramidal coordination, magnetic properties

1. Introduction

Layered oxide materials with the $YbFe_2O_4$ – crystal structure (space group $R\bar{3}m$) exhibit a variety of interesting physical properties that can be tuned through cation substitutions into the octahedral or trigonal bipyramidal sites [1,2]. Structural changes as a result of a substitution are generally observed according to a change in the ionic radii or a change in the electronic interactions, such as with a Jahn-Teller distortion. In contrast to either of the defined structural changes observed with cation substitutions, the substitution of Mg^{2+} into $InGaCuO_4$ has recently been witnessed to produce an unexpected increase in the *c* lattice parameter. It was determined that the large structural change was a result of the dilution of the half filled d_{z^2} orbital of the TBP site, and the removal of the 3*d* electrons from Cu^{2+} produced an expansion of the *c* lattice parameter [3].

Isostructural to $YbFe_2O_4$, $InGaCuO_4$ is defined as a stacking of a single layer of InO_6 octahedra and a double layer of disordered MO_5 (M = Ga^{3+}, Cu^{2+}) trigonal bipyramids (TBP) [2,4]. In comparison to the hexagonal $YMnO_3$ compounds, the TBP site in $InGaCuO_4$ does not have equidistant axial M – O bonds because of the unequal bonding environments between the double MO_5 layers, displayed in Figure 1 [3]. In order to further understand the role of the electronic configuration of the cations in the TBP site, additional cations with similar ionic radii need to be studied.

Kimizuka *et al.* have extensively studied the $A^{3+}Fe^{3+}M^{2+}O_4$ (A^{3+} = Ln, Y, In, and M^{2+} = Cr, Mn, Fe, Co, Ni, Cu, Zn) family of compounds and found that the structure of a compound was commonly influenced by the ionic radii of the cations in the octahedral and TBP sites [1,2]. The study concluded that, in general, a combination of relatively larger A^{3+} and M^{2+} cations would lead to the $YbFe_2O_4$ hexagonal structure, whereas the combination of smaller A^{3+} and M^{2+}

cations would lead to the spinel structure [2]. One anomaly to these observations is apparent when comparing the hexagonal $InFeCuO_4$ phase and the spinel $InFeMgO_4$ phase, where the ionic radii of Cu^{2+} and Mg^{2+} are 0.65 Å and 0.66 Å, respectively [5]. This anomaly can be attributed to the crystal field stabilization for Cu^{2+} in TBP coordination. It has been reported that the $YbFe_2O_4$ – type structure can be described as the low temperature phase, while the spinel structure is the stable high temperature phase for some of the $A^{3+}Fe^{3+}M^{2+}O_4$ compounds, but this temperature – dependent transformation is not observed for either $InFeCuO_4$ or $InFeMgO_4$ [2].

In this paper, the structural, dielectric and magnetic properties of the $InGa_{1-x}Fe_xCuO_4$, $InFeCu_{1-x}Mg_xO_4$, and $InGa_{1-x}Fe_xCu_{1-x}Mg_xO_4$ solid solutions have been studied. The ions of Ga^{3+} (0.55 Å), Fe^{3+} (0.58 Å), Cu^{2+} (0.65 Å) and Mg^{2+} (0.66 Å) were chosen based on the diversity of electronic configurations and similarity in ionic radii [5]. Although Fe^{3+} has an unpaired electron in the d_{z^2} orbital of the TBP site, similar to Cu^{2+} and shown in Figure 2, the electronic interactions of the five unpaired electrons proved to be less influential to the physical properties of $InGaCuO_4$ than the single unpaired electron in the d_{z^2} orbital.

2. Experimental

Polycrystalline samples of $InGa_{1-x}Fe_xCuO_4$ (x = 0 – 1), $InFeCu_{1-x}Mg_xO_4$ (x = 0 – 1) and $InGa_{1-x}Fe_xCu_{1-x}Mg_xO_4$ (x = 0 – 1) were prepared using standard solid state reactions with In_2O_3 (99.99%), Ga_2O_3 (99.999%), Fe_2O_3 (99.99%), CuO (99.99%), and MgO (99.95%). To synthesize the compositions of $InGa_{1-x}Fe_xCuO_4$ (x = 0 – 1) and $InGa_{1-x}Fe_xCu_{1-x}Mg_xO_4$ (x = 0 – 1), stoichiometric amounts of each oxide were intimately mixed under ethanol, pelletized, and then heated at 1150 °C for 24 h with intermediate grindings. The compositions of $InFeCu_{1-x}Mg_xO_4$ (x

= 0 – 1) were synthesized using similar procedures, with a reaction temperature of 1050 °C for the copper – rich compositions and 1200 °C for the magnesium – rich compositions.

Powder X-ray diffraction (XRD) data were obtained on all samples with a RIGAKU MINIFLEX II diffractometer over 5 – 80° 2θ using Cu K_α radiation and a graphite monochromator on the diffracted beam. Lattice parameters were refined through the Le Bail method [6] using the GSAS software and EXPGUI user interface [7,8]. For the compound $InFeCuO_4$, time-of-flight (TOF) powder neutron diffraction data were collected using the POWGEN (BL – 11A) neutron powder diffractometer at the Spallation Neutron Source at Oak Ridge National Laboratory, Oak Ridge, TN [9]. A 5.68 g sample was contained in a 8 mm diameter vanadium sample can and analyzed at 300 K over a *d* – spacing range of 0.301 – 3.108 Å. Rietveld refinements of the data employed the GSAS software and EXPGUI interface [7,8]. The TOF peak-profile function number 3 (a convolution of back-to-back exponentials with a pseudo-Voigt) and the Reciprocal interpolation function were used to model the diffraction peak profiles and backgrounds, respectively.

Zero field cooled (ZFC) DC magnetism data were collected on all hexagonal phase pure samples with a Quantum Design Physical Properties Measurement System (PPMS) using the ACMS mode with a magnetic field of 0.50 Tesla from 3 to 300 K.

3. Results and Discussion

3.1 Structural evolution with Fe^{3+} and Mg^{2+} substitution

XRD patterns obtained for the compositions of $InGa_{1-x}Fe_xCuO_4$ (x = 0 – 1) are shown in Figure 3a. For each composition, all of the diffraction peaks can be indexed with the space group $R\bar{3}m$, and no impurity phases are visible. A complete solid solution between the layered

hexagonal phases $InGaCuO_4$ and $InFeCuO_4$ is therefore evidenced for the first time, to the best of our knowledge. The cell parameter evolution through the solid solution is shown in Figure 3b, where there are appears to be limited changes in the *a* and *c* parameters, which is in agreement with the ionic radii of Ga^{3+} and Fe^{3+}. In order to determine if there is a true change in the lattice parameters as a result of this substitution, further analysis through a comparison with a silicon standard is required.

The XRD patterns of $InFeCu_{1-x}Mg_xO_4$ (x = 0 – 1) are provided in Figure 4a. For the compositions of x = 0 – 0.4, all of the diffraction peaks can be indexed with the same space group, $R\bar{3}m$. The peaks of the diffraction pattern for the compositions of x = 0.8, 0.9, and 1 can be indexed with the $Fd\bar{3}m$ space group corresponding to the spinel phase. With Mg^{2+} concentrations of x = 0.5 – 0.7, the peaks of the diffraction pattern can be successfully indexed with the use of the two above-mentioned space groups, indicating the coexistence of a hexagonal and a spinel phase. The addition of Mg^{2+} into the TBP site causes a shift in the XRD peak positions similar to that observed in $InGaCu_{1-x}Mg_xO_4$ [3], but when the concentration of Mg^{2+} exceeds x = 0.4, diffraction peaks from the spinel $InFeMgO_4$ phase coexists with the hexagonal $InFeCuO_4$ phase until x = 0.8. The *a* and *c* parameters of the hexagonal $InFeCuO_4$ phase follow a linear trend, shown in Figure 4b, where there is an increase in the *c* parameter and a small decrease in the *a* parameter. The solid solution of the hexagonal phase is observed until the Mg^{2+} content reaches x = 0.4. The *a* lattice parameter of the spinel phase for x = 0.8, 0.9 and 1 were refined to be 8.625 Å, 8.647 Å and 8.644 Å, respectively (average ESD: 0.0002).

The XRD patterns of $InGa_{1-x}Fe_xCu_{1-x}Mg_xO_4$ (x = 0 – 1) are shown in Figure 5a. Similar to the samples of $InFeCu_{1-x}Mg_xO_4$, the peaks of the diffraction patterns can be indexed with the space group $R\bar{3}m$ for x = 0 – 0.6 and with the space group $Fd\bar{3}m$ for x = 1. The use of both

mentioned space groups was necessary to successfully index the peaks of the diffraction patterns for $x = 0.7 – 0.9$. The evolution of the hexagonal *a* and *c* axis cell parameters are shown in Figure 5b. The *c* axis parameter linearly increases as Fe^{3+}/Mg^{2+} content increases, which was expected as seen in the previous study of $InGa_{1-x}Fe_xCuO_4$, $InFeCu_{1-x}Mg_xO_4$, and $InGaCu_{1-x}Mg_xO_4$ [3]. The *a* axis lattice parameter remains fairly constant through the complete composition range. This result can be explained regarding the opposing changes occurring in the previous solid solutions: *a* slightly increases in $InGa_{1-x}Fe_xCuO_4$, but slightly decreases in $InFeCu_{1-x}Mg_xO_4$ and $InGaCu_{1-x}Mg_xO_4$ [3]. The solid solution of the hexagonal phase is observed until the Mg^{2+} content reaches $x = 0.7$.

The addition of Fe^{3+} was hypothesized to decrease the *c* axis of the $InGa_{1-x}Fe_xCuO_4$ crystal lattice, which would be analogous to the compression of the *c* axis that was observed as a result of the substitution of Cu^{2+} for Mg^{2+} in $InGaCu_{1-x}Mg_xO_4$ [3]. Unlike the dilution of Cu^{2+}, the *c/a* values of the $InGa_{1-x}Fe_xCuO_4$ compounds are invariable, as it is shown in Figure 6. The constant *c/a* ratio can be explained by further examining the electronic configuration of Fe^{3+}. All of the five *d* electrons from the Fe^{3+} (d^5 – high spin) are unpaired in comparison to the one unpaired electron that is present in the d_{z^2} orbital of Cu^{2+}, Figure 2. This even distribution of unpaired electrons in the *d* orbitals leads to a small expansion of the entire crystal structure, in comparison to the isotropic compression that is produced from the d^9 configuration. These results confirm that the electronic configurations, and specifically the electron pairing, of the cations in the TBP site have a great amount of influence over the structural parameters of these materials. The *c/a* ratio of the hexagonal phase for both $InFeCu_{1-x}Mg_xO_4$ and $InGa_{1-x}Fe_xCu_{1-x}Mg_xO_4$ follow a linear trend that agrees with the dilution of Cu^{2+} observed in $InGaCu_{1-x}Mg_xO_4$,

but the slope of this trend is not as drastic given the interactions of the unpaired *d* electrons of Fe^{3+} in comparison to Ga^{3+} [3].

3.2 Neutron diffraction of the $InFeCuO_4$ hexagonal phase

A Rietveld refinement was completed for the neutron diffraction data collected for a sample of $InFeCuO_4$ in the $R\bar{3}m$ space group starting from the parameters reported for $InGaCuO_4$ (Figure 7) [7,8]. To the best of our knowledge, this is the first reported structural description on $InFeCuO_4$ from neutron diffraction. The In^{3+} site was constrained to be fully occupied, and the refined occupancies of the M site agree with the nominal composition of equal Fe^{3+} and Cu^{2+} concentrations. As with other double layer AM_2O_4 – type compounds, the bond angles of the TBP site indicate an umbrella-type arrangement, where the M cations are displaced slightly above or below the plane of the O2 atoms [3]. The structural and geometric parameters are provided in Tables 1 and 2.

3.3 Magnetic investigation of hexagonal phases

DC – magnetism was collected for all hexagonal phase – pure samples from 3 – 300 K and each sample was corrected for core diamagnetization [10]; which included the compositions of $InGa_{1-x}Fe_xCuO_4$ (x = 0 – 1), $InFeCu_{1-x}Mg_xO_4$ (x = 0 – 0.4), and $InGa_{1-x}Fe_xCu_{1-x}Mg_xO_4$ (x = 0 – 0.6). The zero – field cooled (ZFC) magnetic susceptibility is provided in Figures 8 – 10, where the Curie – Weiss law can be employed with the paramagnetic high temperature region of the $1/\chi$ data (250 – 300 K). The paramagnetic region of the inverse susceptibility plots were used to calculate the Weiss temperatures, $|\theta_w|$, and magnetic moments, $\mu_{eff.}$, for each composition, these values are provided in Table 3. The theoretical magnetic moments were calculated using the

spin values for high-spin Fe^{3+} (d^5, S = 5/2) and Cu^{2+} (d^9, S = 1/2) in the TBP site; the low-spin value for Fe^{3+} had a much lower agreement to the experimental values when compared to the high-spin calculation.

As seen with the $InGaCu_{1-x}Mg_xO_4$ solid solution, the dilution of the magnetic ions in $InFeCu_{1-x}Mg_xO_4$ is verified through a decrease in the experimental magnetic moment [3]; however, it is also noted that for samples within the $InFeCu_{1-x}Mg_xO_4$ solid solution the $1/\chi$ plots show reduced linearity in the high temperature paramagnetic region as Mg content is increased. Two broad peaks are observed in the magnetic susceptibility for $x = 0.2 – 0.4$, and it is possible that one peak is the result of a slight $InFeMgO_4$ spinel impurity. The spinel $InFeMgO_4$ phase has been reported to have a magnetic ordering transition at 23 K, which was determined to be the result of possible ferrimagnetic interactions [11]. Although reflections from the $InFeMgO_4$ phase are not apparent in the present XRD data, the additional peaks in the magnetic susceptibility from the possible impurity spinel phase will be investigated.

For the solid solution $InGa_{1-x}Fe_xCuO_4$, the Weiss and magnetic ordering temperatures observed for the two end members $InGaCuO_4$ and $InFeCuO_4$ agree well with those reported previously [12]. Across the solid solution the strength of the antiferromagnetic (AFM) interactions increase, as indicated in the significant increase in the Weiss temperature, $|\theta_w|$, when Ga^{3+} is substituted for Fe^{3+}. In the case of $InFeCuO_4$, it has previously been suggested that the observation of thermal remnant magnetization may indicate the presence of ferrimagnetism; however, a shift in AC susceptibility transition temperature with frequency was also observed, indicating spin glass type behavior [12]. Across the $InGa_{1-x}Fe_xCuO_4$ solid solution there is a continuous increase in the observed magnetic transition temperature, but for both $InGa_{1-x}Fe_xCuO_4$ and $InGa_{1-x}Fe_xCu_{1-x}Mg_xO_4$ solid solutions the strongest magnetic transitions are

observed at x = 0.4 and x = 0.6 compositions. AC susceptibility measurements were performed at 1000 Hz to further investigate the origin of these transitions for $InGa_{1-x}Fe_xCuO_4$ x = 0.4 and 0.6 samples (Figure 11). The presence of the χ" component says relaxation processes are at play, likely indicating that the low temperature ordering is due to spin glass formation not AFM long range ordering [13].

3.4 Dielectric investigation of hexagonal phases

Dielectric measurements of these materials were attempted, but the samples showed an extremely large amount of dielectric loss because of their semiconducting behavior (approximately 10^6 Ωcm). This semiconductivity can be explained by the suggested mechanism for a similar layered compound, $InGaZnO_4$. Through theoretical calculations, it has been reported that the overlapping In 5*s* orbitals located at the edge of the conduction band is the source of conductivity in these materials [14,15].

4. Conclusion

Substitutions of Fe^{3+} and Mg^{2+} were investigated in the layered $InGaCuO_4$ system where Ga^{3+} and Cu^{2+} are equally distributed in the trigonal bipyramidal site. A complete solid solution was evident for $InGa_{1-x}Fe_xCuO_4$, whereas single phase samples of $InFeCu_{1-x}Mg_xO_4$ and $InGa_{1-x}Fe_xCu_{1-x}Mg_xO_4$ were obtained for x < 0.5 and 0.7, respectively. For higher Fe/Mg content, a mixture of the $InGaCuO_4$ hexagonal phase and the $InFeMgO_4$ spinel phase was obtained. The differences in the electronic configurations of Ga^{3+}, Fe^{3+}, Cu^{2+}, and Mg^{2+} led to transformations that were observed in the structural parameters and magnetic susceptibility. This data has

verified that both the electronic environment and a change in the ionic radii of the cation are significantly influential to altering the physical properties of a material.

Acknowledgements:

This work was supported by NSF Grant DMR 0804167. We thank Ashfia Huq at the Oak Ridge National Lab for her assistance with the neutron data collection and analysis. We would also like to thank Dr. Jun Li at Oregon State University for her assistance and fruitful discussions concerning the structural refinements. This research at Oak Ridge National Laboratory's Spallation Neutron Source was sponsored by the Scientific User Facilities Division, Office of Basic Energy Sciences, U.S. Department of Energy under contract DE-AC05-00OR22725 with UT Battelle, LLC.

References

[1] N. Kimizuka, T. Mohri, Journal of Solid State Chemistry 60 (1985) 382–384.
[2] N. Kimizuka, T. Mohri, Journal of Solid State Chemistry 78 (1989) 98–107.
[3] R. Grajczyk, K. Biswas, R. Berthelot, J. Li, A.W. Sleight, M.A. Subramanian, J. of Solid State Chem. 187 (2012) 258–263.
[4] A. Roesler, D. Reinen, Zeitschrift Fuer Anorganische and Allgemeine Chemie 479 (1981) 119–124.
[5] R.D. Shannon, Acta Cryst A 32 (1976) 751–767.
[6] A. Le Bail, Powder Diffraction 20 (2005) 316–326.
[7] A.C. Larson, R.B. Von Dreele, Los Alamos National Laboratory Report LAUR 86-748 (1994).
[8] B.H. Toby, J. Appl. Cryst. 34 (2001) 210–213.
[9] A. Huq, J.P. Hodges, O. Gourdon, L. Heroux, Z. Kristallogr. Proc. 1 (2011) 127–135.
[10] G. Bain, J. Berry, Journal of Chemical Education 85 (2008) 532–536.
[11] M. Matvejeff, J. Lindén, T. Motohashi, M. Karppinen, H. Yamauchi, Solid State Communications 144 (2007) 249–254.
[12] K. Yoshii, N. Ikeda, Y. Okajima, Y. Yoneda, Y. Matsuo, Y. Horibe, S. Mori, Inorg. Chem. 47 (2008) 6493–6501.
[13] J.A. Mydosh, Spin Glasses, Taylor & Francis, Bristol, PA, 1995.
[14] M. Orita, H. Tanji, M. Mizuno, H. Adachi, I. Tanaka, Phys. Rev. B 61 (2000) 1811–1816.
[15] I. Kang, C. Park, J. of Korean Phys. Soc. 56 (2010) 476–479.

Tables.

Table 1.
TOF neutron diffraction structure refinement of $InFeCuO_4$ [1-4]

	In (3a)	M (6c)	O1 (6c)	O2 (6c)
z	0	0.2141(1)	0.2922(1)	0.1292(1)
U_{11} (Å^2)	0.37(1)	0.77(1)	0.75(1)	1.26(1)
U_{33} (Å^2)	1.35(6)	0.77(1)	0.58(1)	1.34(4)
U_{12} (Å^2)	0.18(2)	0.39(1)	0.38(1)	0.63(1)
Occupancy	1	1 [2]	0.99(1)	0.97(1)

1. Structure refinement completed in $R\bar{3}m$ space group, a = 3.374(1) Å, c = 24.870(1) Å, χ^2 = 4.840, R_{wp} = 3.83%, R_p = 8.10%.
2. The x and y fractional coordinates are 0 for all crystallographic sites.
3. Based on an occupancy of In fixed at 1, the occupancies of Fe and Cu refine to 0.54(5), and 0.46(5), respectively.
4. Thermal parameters (U) were multiplied by 100, $U_{11} = U_{22}$, $U_{13} = U_{23} = 0$.

Table 2.
Bond lengths (Å) and angles (˚)

$InFeCuO_4$	
In–O1 (×6)	2.200(1)
M–O1	1.941(1)
M–O2	2.112(1)
M–O2 (×3)	1.964(1)
O1–In–O1	100.12(1)
O1–In–O1	79.88(1)
O1–M–O2	97.30(1)
O2–M–O2	82.70(1)
O2–M–O2	118.41(1)

Table 3. Magnetic data of the hexagonal phase samples [1,2,3]

	$InGa_{1-x}Fe_xCuO_4$			$InGa_{1-x}Fe_xCu_{1-x}Mg_xO_4$		
(x)	$\|\theta_w\|$	μ_{eff} (μB)	μ_{th} (μB)	$\|\theta_w\|$	μ_{eff} (μB)	μ_{th} (μB)
0.00	40	1.80	1.73	40	1.80	1.73
0.10	60	2.55	2.55	50	2.18	2.49
0.20	110	3.09	3.07	80	2.89	3.07
0.30	130	3.35	3.68	100	3.18	3.55
0.40	190	3.76	4.12	130	3.25	3.98
0.50	230	4.02	4.53	95	3.41	4.36
0.60	260	4.21	4.90	160	3.71	4.71

1) From the limited paramagnetic region of the magnetic susceptibility, the Curie-Weiss law was employed for the temperature range of 250 – 300 K. For compositions of $x = 0.70 – 1$, extremely large Weiss constants and disagreements between the experimental and theoretical magnetic moments indicate that the Curie-Weiss law may not be applicable.
2) The data for $InFeCu_{1-x}Mg_xO_4$ is not included because of the paramagnetic region cannot be well defined.
3) Multiphase samples containing both the hexagonal and cubic phases were not analyzed.

Figure Captions:

Figure 1.
$InGaCuO_4$ crystal structure, with a single layer of InO_6 octrahedra (grey) and a double layer of MO_5 trigonal bipyramids (blue). The *M* cation (blue) is shifted from the basal plane of oxygen (green) because of the unique bonding environments of the *M* – O1 and *M* – O2 bonds [3].

Figure 2.
Electronic splitting of the *d* orbitals for high – spin Fe^{3+} and Cu^{2+} in the TBP crystallographic site. The difference in electronic configurations between these two ions produces contrast in the structural parameters and the physical properties.

Figure 3.
(a) XRD patterns for selected compositions of the $InGa_{1-x}Fe_xCuO_4$ solid solution. The evolution of the diffraction peaks indicates that there is a complete solid solution between the hexagonal $InGaCuO_4$ and $InFeCuO_4$ phases. (b) Le Bail refinements (average ESD: 0.001) of the hexagonal *a* and *c* lattice parameters verify that there is very little change in the crystal structure when Fe^{3+} is substituted for Ga^{3+}.

Figure 4.
(a) XRD patterns from selected compositions of the $InFeCu_{1-x}Mg_xO_4$ solid solution. The addition of Mg^{2+} into the TBP site causes a shift in the XRD peak positions similar to that observed in $InGaCu_{1-x}Mg_xO_4$ [3], but both the hexagonal $InFeCuO_4$ phase and the cubic $InFeMgO_4$ phase are apparent for $x = 0.5 – 0.7$. (b) Le Bail refinements (average ESD: 0.001) of the hexagonal *a* and *c* lattice parameters indicate that there is relatively little change in the *a* parameter compared to the increase in the *c* parameter with the substitution of Mg^{2+} for Cu^{2+}. Asterisks indicate multiphase refinements where the sample had a coexistence of the hexagonal and spinel phases.

Figure 5.
(a) XRD patterns from selected compositions of the $InGa_{1-x}Fe_xCu_{1-x}Mg_xO_4$ solid solution. The co-doping of Fe^{3+} and Mg^{2+} into the $InGaCuO_4$ structure produces structural changes similar to those observed in the $InGa_{1-x}Fe_xCuO_4$ and $InFeCu_{1-x}Mg_xO_4$ solid solutions. Peaks from the cubic $InFeMgO_4$ phase are apparent in the XRD pattern after $x = 0.6$. (b) Le Bail refinements (average ESD: 0.001) of the hexagonal *a* and *c* lattice parameters reveal similar trends to that observed in the $InGa_{1-x}Fe_xCuO_4$ and $InFeCu_{1-x}Mg_xO_4$ solid solutions. Asterisks indicate multiphase refinements where the sample had a coexistence of the hexagonal and spinel phases.

Figure 6.
A comparison of the hexagonal *c/a* ratios indicates that the addition of the Mg^{2+} is necessary for an increase in *c* parameter to occur, which was initially observed in $InGaCu_{1-x}Mg_xO_4$ [3]. The linear trends for the *c/a* ratios of $InGaCu_{1-x}Mg_xO_4$ and $InGa_{1-x}Fe_xCuO_4$ indicate complete solid solutions, but the solid solutions are hindered for $InFeCu_{1-x}Mg_xO_4$ and $InGa_{1-x}Fe_xCu_{1-x}Mg_xO_4$ at $x = 0.50$ and 0.70, respectively.

Figure 7.

Neutron diffraction pattern of $InFeCuO_4$ collected at 300 K, where the observed intensity (black circle), calculated intensity (red line), background refinement (green line), *hkl* reflections (black dash) and the difference calculation (blue line) are provided. The refinement verified the nominal composition of Fe^{3+} and Cu^{2+}, in addition to indicating that both oxygen sites are fully occupied.

Figure 8.
DC Magnetic susceptibility for $InFeCu_{1-x}Mg_xO_4$. (a) A magnetic transition is observed for the few hexagonal phase pure compositions. (b) The inverse magnetic susceptibility indicates strong antiferromagnetic interactions through a negative x – intercept for the paramagnetic region of each sample.

Figure 9.
DC Magnetic susceptibility for $InGa_{1-x}Fe_xCuO_4$. (a) A magnetic transition is first apparent in the $InGa_{0.8}Fe_{0.2}CuO_4$ composition, and an increase in the transition temperature is observed with a decrease in χ for $x = 0.2 - 1$ (inset). (b) The inverse magnetic susceptibility indicates strong antiferromagnetic interactions through a negative x – intercept for the paramagnetic region of each sample.

Figure 10.
DC Magnetic susceptibility for $InGa_{1-x}Fe_xCu_{1-x}Mg_xO_4$. (a) A magnetic transition is observed for $x = 0.2 - 0.6$, with an increase in the transition temperature and a decrease in the observed χ (inset). (b) The inverse magnetic susceptibility indicates strong antiferromagnetic interactions through a negative x – intercept for the paramagnetic region of each sample.

Figure 11.
AC Magnetic susceptibility for $InGa_{1-x}Fe_xCuO_4$, $x = 0.4$ and 0.6. (a) The real component (χ') of the susceptibility shows a magnetic transition similar to what was observed in the DC magnetic susceptibility. (b) The imaginary component (χ'') near the transition temperature indicates that the observed transition is the result of spin glass behaviors, not the presence of long range AFM ordering.

Figure 1.

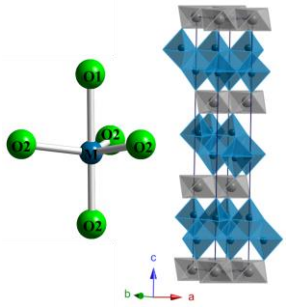

Figure 2.

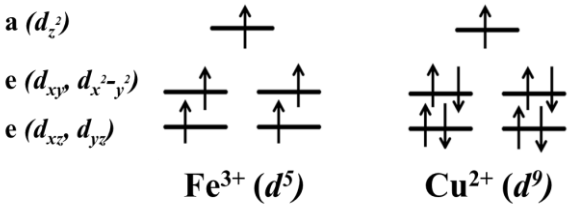

Figure 3.

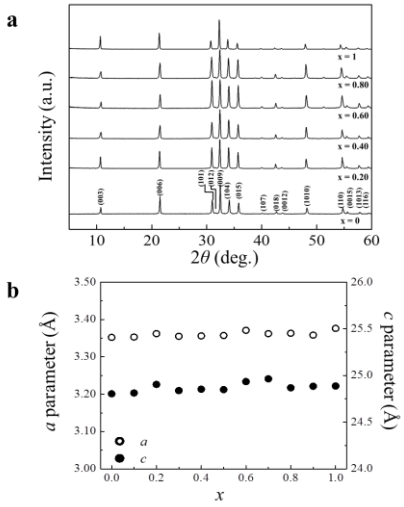

Figure 4.

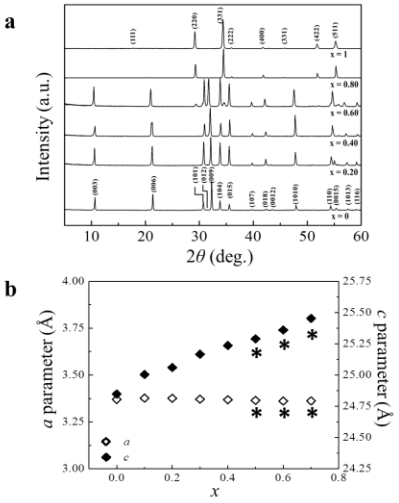

Figure 5.

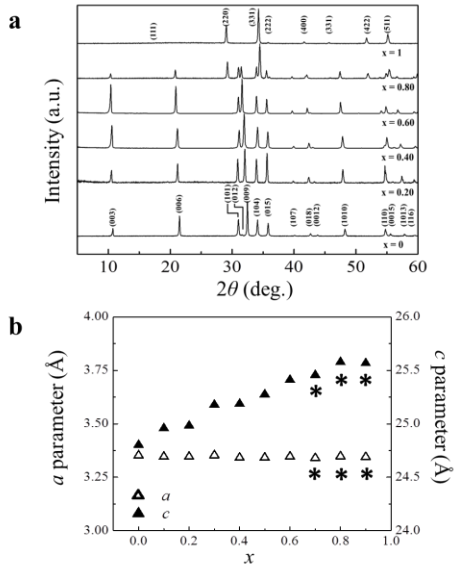

Figure 6.

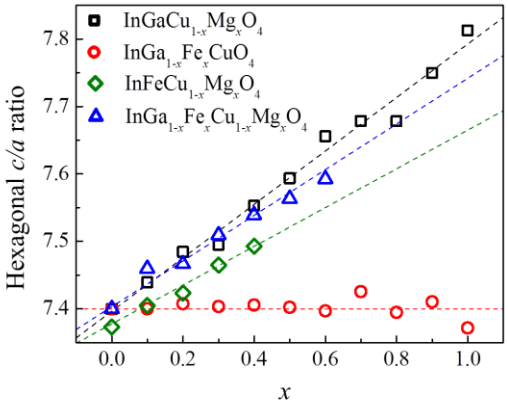

Figure 7.

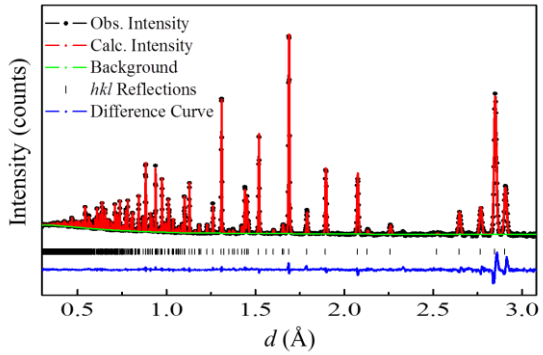

Figure 8.

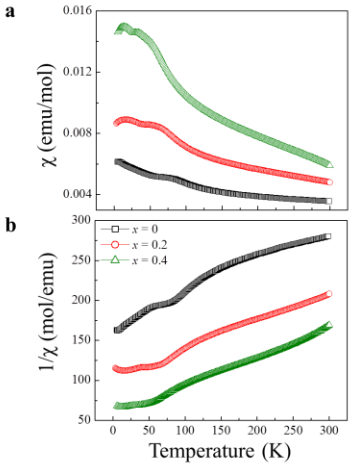

Figure 9.

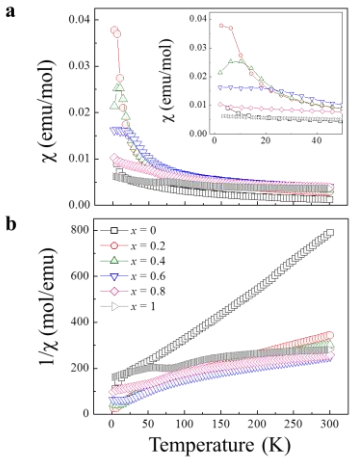

Figure 10.

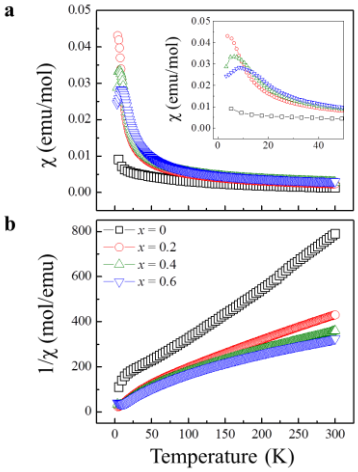

Figure 11.